CrossMark

Improved visible light photocatalytic activity of TiO$_2$ nano powders with metal ions doping for glazed ceramic tiles

Mahnaz Alijani[1] · **Behzad Koozegar Kaleji**[1] · **Sahar Rezaee**[2]

Abstract Self-cleaning and anti-bacterial activities of the photo-catalyst titanium dioxide make it a superior compound for use in the ceramics and glass industry. In order to achieve high self-cleaning efficiency for building products, it is important that Titania is present as anatase phase. Moreover, it is desirable that the particle sizes are in Nano-range, so that a large enough surface area is available for enhanced catalytic performance. In the present paper, Cobalt and Nickel co-doped (4%mol Ni and 4%mol Co doped TiO$_2$) and un-doped TiO$_2$ Nano powders have been prepared by sol–gel technique. They were calcined at the temperatures in the range of 475–1075 °C. Ni/Co co-doped TiO$_2$ postponed the anatase to rutile transformation of TiO$_2$ by about 200–300°C, such that before calcination at 775°C, no rutile was detected for 4 mol% Ni/Co co-doped TiO$_2$. A systematic decreasing on crystallite size and increasing on specific surface area of Ni/Co co-doped TiO$_2$ were observed. Photo-catalytic activity of anatase polymorph was measured by the decomposition rate of methylene blue under visible light. The results showed enhanced catalysis under visible light for Ni/Co co-doped TiO$_2$ as compared to pure TiO$_2$. The enhanced performance was attributed to surface chemistry change associated with a slight shift in the band gap. Depending on the temperatures ranging from 475 to 1075 °C, band gap energy of Ni and Co doped TiO$_2$ crystals decreased. For all samples there is a general reduction of the band gap energy from 3.00 to 2.96 eV.

Keywords Ni/Co co-doped TiO$_2$ · Sol–gel method · Optical band gap energy · Structural properties

✉ Mahnaz Alijani
mahnaz.alijani@icloud.com

Behzad Koozegar Kaleji
b.kaleji@malayeru.ac.ir

1 Department of Materials Engineering, Malayer University, Malayer, Iran

2 Department of Physics, Kermanshah Branch, Islamic Azad University, Kermanshah, Iran

1 Introduction

Introduction Development of self-cleaning materials, understanding their structure–function relationship, and engineering artificial surface swith variable wettability suitable for various commercial applications constitute an active research domain in material science (Liu et al. 2014). One of the most emergent applications of TiO_2 is on glazed ceramic tiles (Raimondo et al. 2012; Ducman et al. 2013; Petrovič et al. 2012).

Titanium dioxide (TiO_2) is an important photo-catalytic material that exists as two main polymorphs, Anatase (Tetragonal, a = 0.3785 nm, c = 0.9514 nm) and rutile (Tetragonal, a = 0.4594 nm, c = 0.29589 nm) (Fisher and Egerton 2001; Peters and Vill 1989; Burdett et al. 1987). The Anatase crystalline phase, which is stable at low temperatures, transform into Rutile by calcination at higher temperatures. However, Anatase can be stabilized at high temperatures in presence of dopants during synthesis which inhibits it transformation into Rutile (Kostov 1973; Shon et al. 2008; Gopal et al. 1997).

Previous reports show that experimental band gap of Anatase ($\sim$3.2 eV, that corresponds to a photon with the wavelength of $\sim$387 nm) larger than rutile ($\sim$3.0 eV, that corresponds to a photon with the wavelength of $\sim$413 nm) (Beltran et al. 2006; Hirano et al. 2003; Riyas et al. 2007; Sun et al. 2003). The photo-catalytic activity of TiO_2 has been found to vary with its structural form and is reportedly higher in Anatase form compared to rutile form (Tsai and Cheng 1997).

Pure TiO_2 is not suitable for in-door self-cleaning surfaces as one of the potential application in the self-clean building materials (Smitha et al. 2010; Fujishima et al. 2008). It is necessary to improve its visible-light activities by extending its absorption threshold from the UV light region to the visible light region.

TiO_2 doped with Ce, V, Cu, Sn, Ni, Fe, Cr, or Co shows a red shift in the absorption band compared to pure TiO_2, and considerable photo-catalytic activity under visible light irradiation (Li et al. 2005; Kubacka et al. 2007; Jin et al. 2007; Ma et al. 2009; Xie and Yuan 2004; Bouras et al. 2007; Kudo 2007). Metal dopants have been used to improve the morphology and photo-catalytic activity of TiO_2.

Among various transition metal ion dopants, Ni^{2+} appears to be a more efficient dopant for TiO_2 as it has improved the photo-catalytic activity of certain semiconductor photo-catalysts (Begum et al. 2008; Sreethawong et al. 2005). Supha et al. (2015) found Ni-doped TiO_2 effectively extended absorption of TiO_2 into the visible light range.

One dopant of interest for photo catalysis and other electromagnetic applications is cobalt. Several techniques have been used for the preparation of Co-doped TiO_2. Siddhapara and Shah (2012) reported for pure TiO_2 the transformation from Anatase to rutile phase takes place at 500 °C whereas for Cobalt doped TiO_2 transition is above 600 °C. It is evident that phase transition at a little higher temperature is caused by structural cobalt doping, the substitution of Ti ion by Cobalt ions in the structural framework.

Here in this study, we have developed a new generation Titania photo-catalyst that was co-doped with cobalt (4% mol) and nickel (4% mol), were prepared via sol–gel method. The effect of the dopant on the stability of Anatase phase and optical properties in high temperature was studied. The presence of Anatase phase at the 700–800 °C would allow the use of Titania powder as a coating in glazed ceramic tiles, particularly for those processes which include a second firing stage at this temperature range for decoration purposes. The efficiency of these samples as photo-catalysts for degradation of MB, an azo dye, under visible light was investigated.

2 Experimental procedures

2.1 Preparation of the nanopowders

TiO_2 sol was firstly prepared according to the method reported in our previous studies (Alijani and Kaleji 2017; Kaleji et al. 2016). Titanium butoxide (liquid) (TBT, $TiO_4C_{16}H_{36}$) with a purity of 99% (Aldrich chemistry) was used as a titanium precursor, ethanol (EtOH), ethyl acetoacetate (EAcAc), which is as a sol stabilizer, and nitric acid (HNO_3) as catalyst. For preparation of Nickel and Cobalt-doped TiO_2 sols, nickle (II) nitrate hexahydrate (Ni $(NO_3)_2 \cdot 6H_2O$, Merck chemistry) and cobalt nitrate (Co $(NO3)2 \cdot 6H2O$, Merck) was dissolved in TiO_2 sol with 4 molar percentage. Ni was doped 20 min after Co doping under continuous stirring at room temperature for 30 min. The formed gel was dried at 100 °C for 60 min. Finally, the prepared samples were calcined at desired temperatures (475, 675,775, 875, 975, 1075 °C) for 1 h (Fig. 1).

2.2 Characterization methods

Thermal analysis (DTA) was used in order to determine crystallization temperature with a heating rate of 10 °C/min (STA 1460 equipment). Powder X-ray diffraction patterns were collected on a Unisantis XMD300 powder diffractometer unit using Cu kα ($\lambda = 1.5418$ Å) at 45 kV and 0.8 Ma using a standard sample holder. The samples were scanned in the 2θ ranging of 20°–70°. The average crystallite size of nanopowders (d) was determined from

Fig. 1 Experimental flow diagram of the TiO_2 doped photo-catalysts
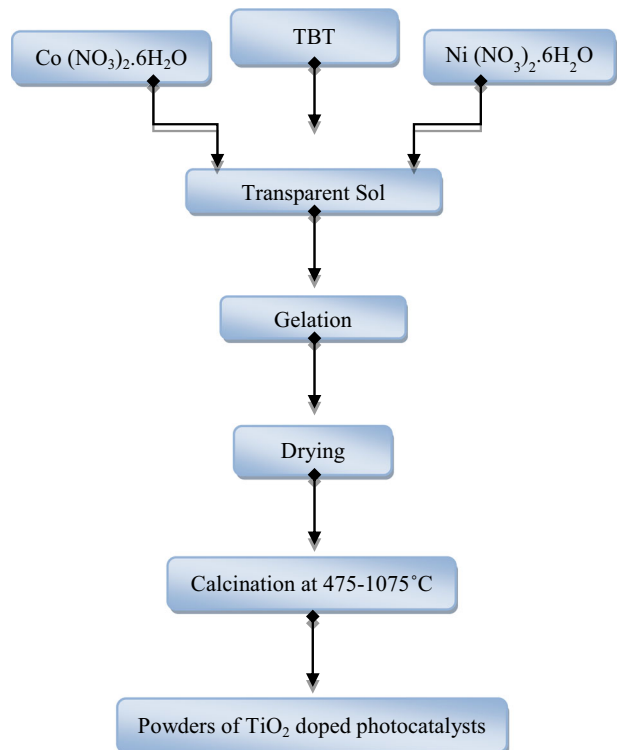
the XRD patterns, according to the Scherrer equation (Ilkhechi et al. 2016; Kaleji et al. 2013).

$$d = k\lambda/\beta\cos\theta \tag{1}$$

where k is a constant (shape factor, about 0.9), λ the X-ray wavelength (0.154 nm), β the full width at half maximum (FWHM) of the diffraction peak, and θ is the diffraction angle. The values of β and θ of anatase and rutile phases were taken from anatase (101) and rutile (110) planes diffraction lines, respectively. The amount of rutile in the samples was calculated using the following equation (Ilkhechi et al. 2016; Kaleji et al. 2013).

$$X_R = (1 + 0.8(I_A/I_R))^{-1} \tag{2}$$

where X_R is the mass fraction of rutile in the samples, I_A and I_R are the X-ray integrated intensities of (101) reflection of the anatase and (110) reflection of rutile, respectively. The diffraction peaks of crystal planes (101), (200), and (105) of anatase phase in XRD patterns were selected to determine the lattice parameters of the TiO$_2$ and doped TiO$_2$ nanopowders. The lattice parameters were obtained by using the Eq. 3 (Ilkhechi et al. 2016; Kaleji et al. 2013).

$$\begin{aligned} (\text{Bragg's law}) : 2d_{(hkl)} \sin\theta = \lambda \\ (1/d_{hkl})^2 = (h/a)^2 + (k/b)^2 + (l/c)^2 \end{aligned} \tag{3}$$

where $d_{(hkl)}$ is the distance between the crystal planes of (h k l); λ is the wavelength of X-ray used in the experiment; θ is the diffraction angle of the crystal plane (h k l); h k l is the crystal plane index; and a, b, and c are lattice parameters (in anatase form, $a = b \neq c$).

Morphology of the nanopowder was observed using the scanning electron microscope (FE-SEM, TESCAN-MIRA3) with an accelerating voltage of 10–30 kV. The samples used for SEM characterization were coated with 5 nm thin layer of Au using the standard sputtering technique. Elemental analysis was carried out using Link, MIRA3, TESCAN, energy dispersive X-ray spectroscopy (EDAX) detector. A Zeiss Technai EM10C transmission electron microscope operating at 80–100 kV was used to record the transmission electron microscopy (TEM) patterns. Nitrogen adsorption isotherms were measured at 77 K using a N$_2$ adsorption analyzer (Bel Japan- BelSORP miniII). The Brunauer, Emmett, and Teller (BET) model was used to estimate the surface area of the samples according to the N$_2$ adsorption data. Fourier transform infrared (FTIR) spectra were recorded using a Perkin-Elmer Spectrum (RXI) spectrophotometer in the range 400–4000 cm^{-1}. Each FTIR spectrum was collected after 20 scans with the resolution of 2 cm^{-1}.

2.3 Band gap energy measurement

The proper amounts of mentioned dispersant (HNO$_3$) was added to 50 ml distilled water followed by the addition of 0.01 g of samples calcined at different temperature for TiO$_2$ and T-4%Ni-4%Co. pH of suspension was adjusted to a desired value, then the suspension was stirred for 30 min using a magnetic stirrer and subjected to a subsequent treatment in an ultrasonic bath for 60 min. Moreover, the dispersion stability of doped and pure TiO$_2$ aqueous suspension was evaluated by the absorbance of suspension using a model lambda 25-perkinelmer UV–Visible spectrometer. UV–Vis spectroscopy techniques, respectively, by following the Tauc's relation [$(\alpha h\nu) = C (h\nu - Eg)^n$], where C is a constant, α is absorption, E_g is the average bandgap of the material and "n" depends on type of transition

(2 for indirect bandgap and 1/2 for direct bandgap), h is the Plank's constant $(6.626 \times 10^{-34}$ J-s), and v is the frequency of photons (Guo et al. 2005; Verma et al. 2005). The direct and indirect average bandgap transition energies were estimated from the intercepts of linear portion of the $(\alpha h v)^2$ or $(\alpha h v)^{1/2}$ versus hv of plots, respectively.

3 Results and discussion

3.1 DTA analysis

Figure 2 can be attributed to the oxidation of the organic substances and Anatase to Rutile phase transformation in pure TiO_2, respectively. The curve shows an endothermic peak at 50–100 °C which is attributed to evaporation of absorbed water and solvent (EtOH) from the gel. The first exothermic peak 120–140 °C is probably attributed to combustion of residual organic component of TBT precursor. It is clear that titania precursor gel is thermally stable from 140 °C up to 280 °C. Small exothermic peak at temperature of 290–340 °C is probably corresponds to combustion of EAcAc (auto ignition temperature: 295 °C). The curve contains two exothermic peaks, first at about 400–470 °C related to the crystallization of anatase phase of TiO_2 and at 495 °C which is related to the phase transformation of anatase to rutile (Kaleji et al. 2016).

3.2 X-ray diffraction studies of the nanopowders

X-ray diffraction measurements were carried out to study the crystal structure and crystalline quality. Figure 3 represents the X-ray diffraction pattern of synthesized pure and Ni and Co co-doped TiO_2 nanoparticles calcined at 475–1075 °C for 1 h. It is revealed that diffraction peaks of the pure sample matches well with those of a standard anatase TiO_2 (JCPDS card number 21-1272) with high crystallinity. The Ni and Co co-doping does not lead to the disappearance of the indexed peaks, proving that the crystallographic structure of the doped samples is similar to that of the pure TiO_2 sample. By comparing the relative
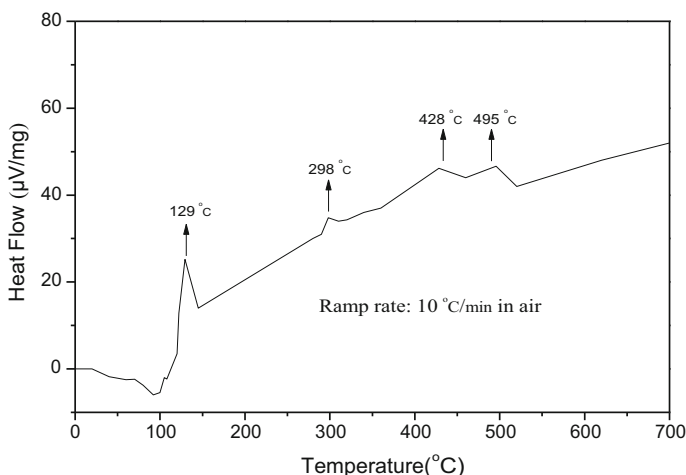

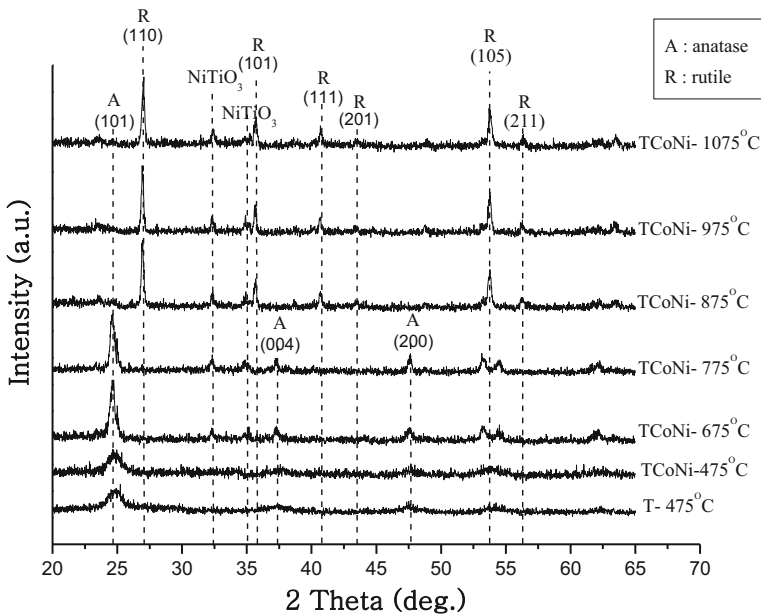**Fig. 2** DTA curve of Titania based precursor gel from ambient temperature up to 700 °C

Fig. 3 XRD patterns of pure TiO_2 and Ni/Co co-doped TiO_2 powders, formed at various temperatures 475–1075 °C for 1 h

intensity of the diffraction peaks, it can be seen that the intensity of (101) plane decreased and the peak position (2θ) is decreased after doping which indicates that dopant cations are successfully doped into TiO_2 crystal lattice. For the T–Ni–Co samples calcined at 475–775 °C, only the main peak of the TiO_2 anatase phase, 25° (2Θ), was barely observable. When calcination temperature was increased to 875–1075 °C, only the rutile (JCPDS card number 21-1276) phase was identified.

The calculated crystallite size and lattice parameter of anatase, calculated by scherrer formula, are reported in Table 1. Based on the XRD data Table 1, the lattice constants a and c of the pure TiO_2 sample was found to be 3.822 Å and 10.660 Å, respectively. For Ni/

Table 1 XRD data doped and TiO_2 nanocrystalline powder

Samples (°C)	Crystal phase	Crystal size	Lattice parameters		$V_{u.c}$ (Å)^3	Surface area BET (m^2 g^{-1})
			a = b	c		
T-475	Anatase	21.8	3.822	10.660	155.717	71.483
TCoNi-475	Anatase	15.5	3.857	9.627	143.215	100.544
TCoNi-675	Anatase	19.1	3.877	9.655	145.125	81.593
TCoNi-775	Anatase	32.7	3.907	9.875	150.738	47.658
TCoNi-875	Rutile	30.3	4.482	2.946	59.180	45.592
TCoNi-975	Rutile	37.6	4.517	2.953	60.250	37.546
TCoNi-1075	Rutile	42.3	4.351	2.985	56.509	33.375

Co co-doped samples, lattice parameter was decreased. According to Vegard's law (Vegard 1921; Jacob et al. 2007), a statistical substitution of Ni/Co dopants within the TiO_2 host lattice leads to a lattice expansion. Their substitution for Ti^{4+} ion will reduce the lattice parameters of the Ni/Co co-doped samples. The Ni^{2+} radius (0.069 nm) is bigger than Ti^{4+} radius (0.061 nm) but Co^{+4} radius (0.058 nm) is smaller than Ti^{+4} and both factors could led to slight induced stress in TiO_2 lattice (Kubacka et al. 2007).

The crystallite size of TiO_2 nanoparticles was determined from the most intense peak (101) using the Scherrer formula. The crystallite size was 21.8 nm for pure nanoparticles, 15.5 nm for Ni/Co co-doped (calcined at 475 °C). The crystallite size of the anatase increased from 21.8 to 32.7 nm when the temperature was raised to 775 °C. The decrease in crystallite size can be attributed to the presence of Ni–O–Ti and Co–O–Ti in the Ni and Co doped TiO_2 nanopowders which inhibits the growth of crystal grains. The crystallite size increases with the annealing temperature. Table 1 shows surface area of the Ni and Co co-doped nanopowders is higher than pure TiO_2. The lattice parameters, cell volume, and surface area have decreased with increase the calcination temperatures for anatase (475–775 °C) and rutile (875–1075 °C) nanoparticles. It is common that the surface area decreases at elevating temperatures (surface $area_{min} = 26.677 \ m^2/g$). With increasing temperature, the particles are simply growing to reduce their free energy (i.e. maximizing the volume to surface ratio). They may also shift from being more amorphous to more crystalline in the process. It should be noticed that besides the XRD peaks that have arisen from the main phase of TiO_2, ≥ 675 °C there were some additional peaks in XRD patterns of the Ni/Co co-doped samples, which were assigned to very minor contents $NiTiO_3$ (JCPDS Card No. 33-0960) or $CoTiO_3$ (JCPDS Card No. 77-1373), as depicted in Fig. 3.

3.3 Photocatalytic activity

Figure 4 shows the results of photocatalytic activities of the pure and co-doped TiO2 powders were examined based on the degradation of MB (5 mg/L) under visible irradiation at different calcination temperatures. All the doped TiO_2 samples were able to degrade the MB much faster than the pure TiO_2 sample. The doped metallic ions may play a very important role in charge separation by capturing the electrons. Ni and Co ions play an important role in trapping the electrons and helps in charge separation; hence
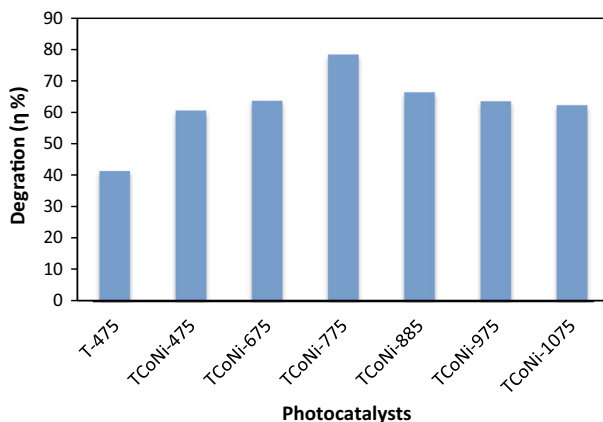

Fig. 4 The photocatalytic activity of pure TiO_2 and Ni/Co co-doped TiO_2 powders

photocatalytic activity is comparatively good. The photocatalytic activity was found to be strongly influenced by the calcination temperatures. Sample TNiCo-775 has the highest rate of decomposition. To improve the photocatalytic properties, optimum mode of both particle size and special level should be considered.

3.4 Optical evaluation

The optical properties of materials are very sensitive to, and are heavily influenced by their inherent microstructures and hence electronic structural changes. UV–vis absorbance experiments were carried out, and the resulting spectra are shown in Fig. 5 The spectrum of the Ni/Co co-doped TiO_2 reported the absorption at the wavelength around 413 nm with the band gap of 3 eV (Table 2), as calculated by the formula E_g (eV) = 1240/λ (nm), where λ stands for the wavelength corresponding to the intersection point of the vertical and horizontal parts of the spectra (Hsieh et al. 2009; Hogarth and Al-Dhhan 1986). The TiO_2 is activated with photons of energy of a longitude close to 400 nm which involves a band gap of 3.2 eV; the literature reports a 3.23 eV value for anatase phase. The absorbance edge in the Ni/Co co-doped TiO_2 powders was significantly shifted to the visible region. This red shift is attributed to the presence of nickel and cobalt in the lattice structure of the TiO_2. This modification serves to alter the electronic band structure. As shown in Fig. 5, indirect energy band gaps were determined by extrapolation of the absorption band to the hν axis. By assuming TiO_2 to be an indirect semiconductor, the
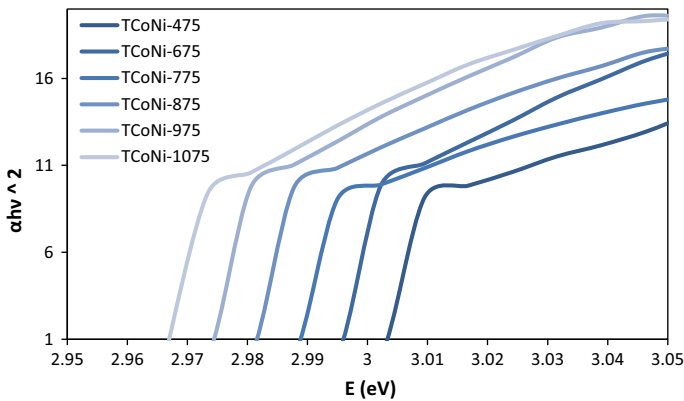
Fig. 5 Tauc plots of Ni/Co co-doped TiO_2 nanopowders calcined at 475–1075 °C for 1 h (direct band gap)

Table 2 Band gap of Ni/Co co doped TiO_2 at variuse tempretures	Sample (°C)	λ_{edge} (nm)	E_g (eV)
	TCoNi-475	413	3
	TCoNi-675	414	2.99
	TCoNi-775	415	2.98
	TCoNi-875	416	2.98
	TCoNi-975	417	2.97
	TCoNi-1075	418	2.96

value of band gap energy of Ni/Co co-doped TiO_2 are 3.00, 2.99, 2.98, 2.98, 2.97 and 2.96 eV for the heating rates of 5 °C/min at different temperature (475–1075 °C), respectively. It has been reported that as the particle size decreases to a certain critical size, its bandgap energy increases (Ilkhechi et al. 2016; Hogarth and Al-Dhhan 1986). It is vision from Table 1 that the band gap decreases with the increase in temperature, while the crystallite size of anatase and rutile phase increases.

3.5 FE-SEM and EDX analysis of pure and doped TiO_2 nanopowders

Morphologies of pure and Ni/Co co-doped TiO_2 calcined at 475 °C are revealed by FE-SEM micrographs and presented here in Fig. 6 It can be seen from Fig. 6b that the doped TiO_2 calcined at 475 °C have slightly lower particles size than pure TiO_2 (Fig. 6a). The pure and doped TiO_2 samples (Fig. 6) are composed of strongly agglomerated nanometric particles, island-like in shape. It can be clearly seen that the microstructures of the powders are strongly affected by doping and calcination temperatures which is due to aggregation of particle size. The EDX data of doped TiO_2 show in Fig. 7 Shows two peaks around 4.5 keV. The intense peaks are assigned to the bulk TiO_2 and the less intense one to the surface TiO_2. Also the peaks of Ni at 6–7 keV and Co at around 7.5–8.5 keV are distinct in Fig. 6 the less intense peak is assigned to dopant in the TiO_2 lattices. These results confirmed the existence of cations in of the solid catalysts.

3.6 Fourier Transform Infrared (FTIR) studies

The FT-IR spectra of pure TiO_2 and Ni/Co co-doped TiO_2 calcined at 475 °C in the range of 400–4000 cm^{-1} are given in Fig. 8 Metal oxides generally give absorption bands in fingerprint region below 1000 cm^{-1} arising from inter-atomic vibrations. The absorption peaks at 3419 and 1638 cm^{-1} appear both in pure TiO_2 and Ni/Co–TiO_2, respectively. The
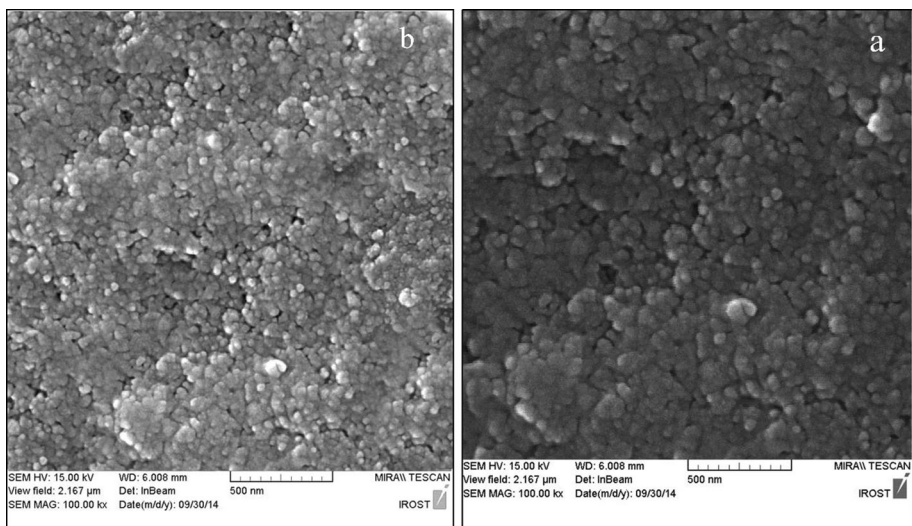

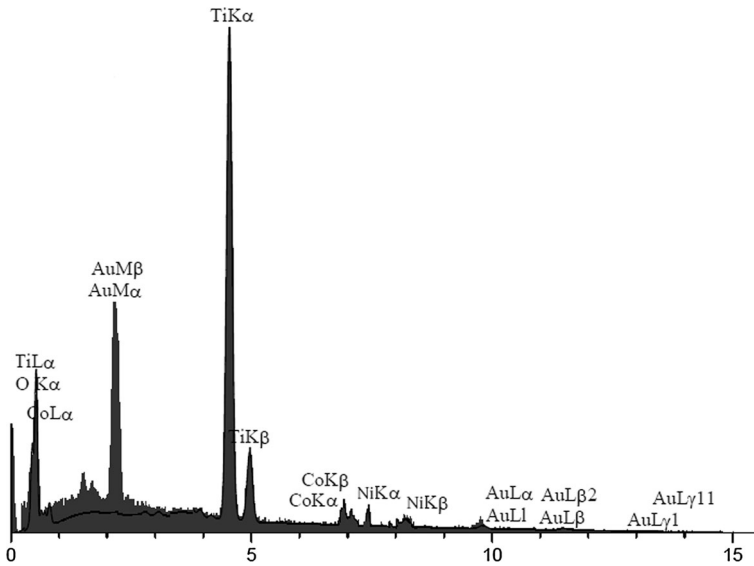**Fig. 6** FE-SEM images of pure (**a**) and doped TiO_2 (**b**), calcination temperature at 475 °C

Fig. 7 Energy dispersive X-ray (EDX) spectra of Ni/Co co-doped TiO_2 calcination temperature at 475 °C

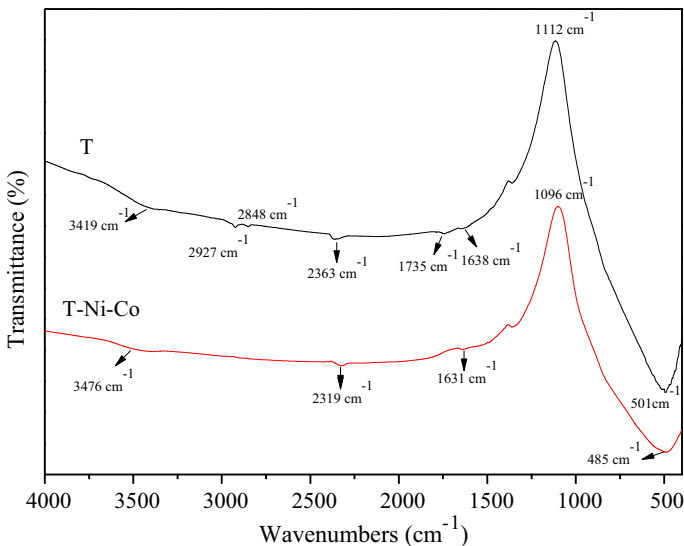**Fig. 8** FTIR spectra for the as-prepared undoped TiO_2 and Ni/Co co-doped TiO_2 calcination temperature at 475 °C

absorption peaks at 3419 and 3476 cm^{-1} is the result of O–H stretching modes which originate from the surface water molecule; these are related to the physical absorption of water (Mul et al. 2001; Du et al. 2008). The –OH bending modes, which originate from the surface of TiO_2, are located at near 1600 cm^{-1}. As known, the hydroxyl groups can improve the photocatalytic activity (Liao et al. 2004; Hong and Kang 2006). The peaks in
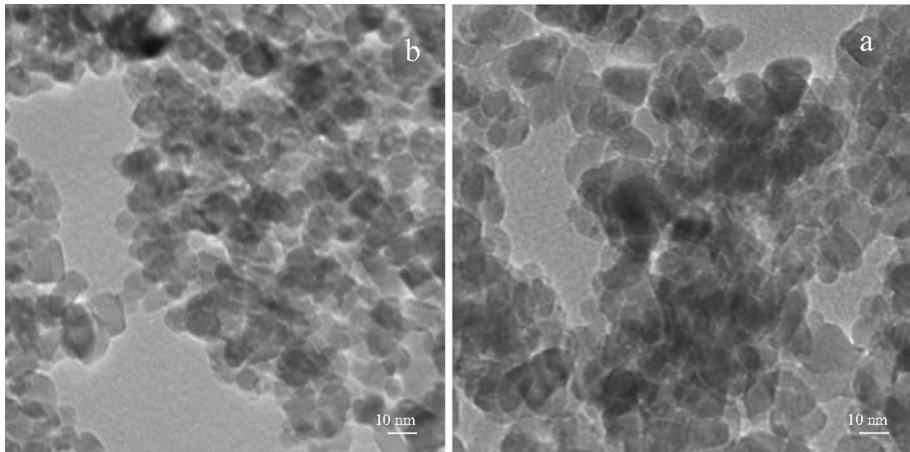
Fig. 9 TEM micrograph of TiO_2 and T-Ni-Co calcined at 475 °C: **a** TiO_2, **b** co-doped TiO_2 nanoparticles

between 2927 and 2848 cm^{-1} were assigned to C–H stretching vibrations of alkane groups. The alkane and carboxylic groups come from titanium (IV) butoxide and ethanol (precursor material), when we used in the synthesis process. There are characteristic wide peaks in the region 1000–500 cm^{-1}, which are related to the bending vibration of the Ti–O bonds (Kumaresan et al. 2011; Riaz et al. 2012; Karthik et al. 2010). When metal ions are doped to the surface of TiO_2, the absorption band significantly transforms and simultaneously new absorption band appears.

3.7 TEM studies of pure and doped TiO_2 nanopowders

The particle morphologies of pure TiO_2 and Ni/Co co-doped TiO_2 were observed by TEM, and micrographs were shown in Fig. 9 The Ni/Co co-doped particles (Fig. 9b) are more disperse than pure TiO_2 (Fig. 9a) with smaller particle sizes. In Fig. 8a, b, the particle sizes of pure TiO_2 and Ni/Co co-doped TiO_2 were around 5–25 and 5–15 nm with the narrow particle size distribution. These are consistent with the XRD results.

4 Conclusions

In this research, pure TiO_2 and Ni/Co co-doped TiO_2 nanoparticles have been prepared by sol–gel technique. The effects of calcination temperature (475–1075 °C) and metal ion doping on the transformation of anatase to rutile phase, crystallite size and optical properties of Titania nanopowders has been investigated. The presence of Ni(II) and Co(III) ions doping in the TiO_2 nanostructure has a significant effect on the transformation of anatase to rutile phase. Based on XRD patterns, the anatase to rutile phase transformation was inhibited by Co/Ni co-doping. Ni and Co inhibited the growth of crystallite size of anatase and the amorphous anatase transformation as well as the subsequent anatase–rutile transformation. The averages particle sizes of the prepared samples varied from 15 to 42 nm with increase in calcination temperature.

Optical properties of TiO$_2$ are greatly influenced by its crystallinity, grain size, surface areas, and surface hydroxyl content.

References

Alijani, M., Kaleji, B.K.: Optical and structural properties of TiO$_2$ nanopowders with Ce/Sn doping at various calcination temperature and time. Opt. Quant. Electron. **49**(1), 34 (2017)

Begum, N.S., Ahmed, H.F., Gunashekar, K.R.: Synthesis of nanocrystalline TiO$_2$ thin films by liquid phase deposition technique and its application for photocatalytic degradation studies. Bull. Mater. Sci. **31**(5), 747–751 (2008)

Beltran, A., Gracia, L., Andres, J.: Density functional theory study of the brookite surfaces and phase transitions between natural titania polymorphs. J. Phys. Chem. B **110**, 23417–23423 (2006)

Bouras, P., Slathatos, E., Lianos, P.: Pure versus metal-ion-doped nanocrystalline titania for photocatalysis. Appl. Catal. B Environ. **73**, 51–59 (2007)

Burdett, J.K., Hughbanks, T., Miller, G.J., Richardson, Jr, J.W., Smith, J.V.: Structural-electronic relationships in inorganic solids: powder neutron diffraction studies of the rutile and anatase polymorphs of titanium dioxide at 15 and 295 K. J. Am. Chem. Soc. 109(12):3639–3646 (1987)

Du, P., Bueno-Lopez, A., Verbaas, M., Almeida, A.R., Mul, G.: The effect of surface OH-population on the photocatalytic activity of rare earth-doped P25-TiO$_2$ in methylene blue degradation. J. Catal. **260**, 75–80 (2008)

Ducman, Vilma, Petrovič, Vladimira, Škapin, Srečo D.: Photo-catalytic efficiency of laboratory made and commercially available ceramic building products. Ceram. Int. **39**(3), 2981–2987 (2013)

Fisher, J., Egerton, T.A.: Titanium Compounds, Inorganic, Kirk-Othmer Encyclopaedia of Chemical Technology. Wiley, New York (2001)

Fujishima, A., Zhang, X., Tryk, D.A.: TiO$_2$ photocatalysis and related surface phenomena. Surf. Sci. Rep. **63**, 515–582 (2008)

Gopal, M., Chan, W., Jonghe, L.: Room temperature synthesis of crystalline metal oxides. J. Mater. Sci. **32**, 6001–6008 (1997)

Guo, B., Liu, Z., Hong, L., Jiang, H.: Sol gel derived photocatalytic porous TiO$_2$ thin films. Surf. Coating Technol. **198**, 24–29 (2005)

Hirano, M., Nakahara, N., Ota, K., Tanaike, O., Inagaki, N.: Photoactivity and phase stability of ZrO$_2$-doped anatase-type TiO$_2$ directly formed as nanometer-sized particles by hydrolysis under hydrothermal conditions. J. Solid State Chem. **170**(1), 39–47 (2003)

Hogarth, C.A., Al-Dhhan, Z.T.: Optical absorption in thin films of cerium dioxide and cerium dioxide containing silicon monoxide. Physica Status Solidi (B) **137**(2), 1157–1160 (1986)

Hong, W.J., Kang, M.: The super-hydrophilicities of Bi–TiO$_2$, V–TiO$_2$, and Bi–V–TiO$_2$ nano-sized particles and their benzene photodecompositions with H$_2$O addition. J Mater Lett. **60**, 1296–1305 (2006)

Hsieh, C.T., Fan, W.S., Chen, W.Y., Lin, J.Y.: Adsorption and visible-light-derived photocatalytic kinetics of organic dye on Co-doped titania nanotubes prepared by hydrothermal synthesis. Sep. Purif. Technol. **67**, 312–318 (2009)

Ilkhechi, N.N., Alijani, M., Kaleji, B.K.: Optical and structural properties of TiO$_2$ nanopowders with Co/Ce doping at various temperature. Opt. Quant. Electro **48**(2), 1–9 (2016)

Jacob, K.T., Raj, Shubhra, Rannesh, L.: Vegard's law: a fundamental relation or an approximation? Int. J. Mater. Res. **98**(9), 776–779 (2007)

Jin, Z., Zhang, X., Li, Y., Li, S., Lu, G.: 5.1% Apparent quantum efficiency for stable hydrogen generation over eosin-sensitized CuO/TiO$_2$ photocatalyst under visible light irradiation. Catal. Commun. **8**, 1267–1273 (2007)

Kaleji, B.K., Hosseinabadi, N., Fujishima, A.: Enhanced photo-catalytic activity of TiO$_2$ nanostructured thin films under solar light by Sn and Nb co-doping. J. Sol-Gel. Sci. Technol. **65**(2), 195–203 (2013)

Kaleji, B.K., Alijani, M., Aghaei, A.: Sn/Ce co-doping of TiO$_2$. J. Mater. Sci. Mater. Electron. **27**(8), 8524–8531 (2016)

Karthik, K., Pandian, S.K., Jaya, N.V.: Effect of nickel doping on structural, optical and electrical properties of TiO$_2$ nanoparticles by sol–gel method. Appl. Surf. Sci. **256**, 6829–6833 (2010)

Kostov, I.: Minerology, 3rd edn. Nauka, Izkustia (1973)

Kubacka, A., Fuerte, A., Martinez-Arias, A., Fernandez-Garcia, M.: Nanosized Ti–V mixed oxides: effect of doping level in the photo-catalytic degradation of toluene using sunlight-type excitation. Appl. Catal. B Environ. **74**, 26–33 (2007)

Kudo, A.: Recent progress in the development of visible light-driven powdered photocatalysts for water splitting. Int. J. Hydrog. Energy 32, 2673–2678 (2007)

Kumaresan, L., Prabhu, A., Palanichamy, M., Arumugam, E., Murugesan, V.: Synthesis and characterization of Zr 4 + , La 3 + and Ce 3 + doped mesoporous TiO_2: evaluation of their photocatalytic activity. J. Hazard. Mater. 186, 1183–1192 (2011)

Li, F.B., Li, X.Z., Hou, M.F., Cheah, K.W., Choy, W.C.H.: Enhanced photocatalytic activity of Ce 3 + – TiO_2 for 2-mercaptobenzothiazole degradation in aqueous suspension for odour control. Appl. Catal. A Gen. 285, 181–189 (2005)

Liao, S., Donggen, H., Yu, D., Su, Y., Yuan, G.: Preparation and characterization of ZnO/TiO_2, $SO_4^{2-}/ZnO/TiO_2$ photocatalyst and their photocatalysis. J. Photochem. Photobiol. A: Chem. 168(1), 7–13 (2004)

Liu, Kesong, Cao, Moyuan, Fujishima, Akira, Jiang, Lei: Bio-inspired titanium dioxide materials with special wettability and their applications. Chem. Rev. 114(19), 10044–10094 (2014)

Ma, T.Y., Cao, J.L., Shao, G.S., Zhang, X.J., Yuan, Z.Y.: Hierarchically structured squama-like cerium-doped titania: synthesis, photoactivity, and catalytic CO oxidation. J. Phys. Chem. C 113, 16658–16667 (2009)

Mul, G., Zwijnenburg, A., van der Linden, B., Makkee, M., Moulijn, J.A.: Stability and selectivity of Au/TiO_2 and $Au/TiO_2/SiO_2$ catalysts in propene epoxidation: an in situ FT-IR study. J. Catal. 201, 128–137 (2001)

Peters, G., Vill, V.: Index of Modern Inorganic Compounds. Subvolume A. Landolt-Börnstein Numerical Data and Functional Relationships in Science and Technology. Verlag, Berlin (1989)

Petrovič, Vladimira, Ducman, Vilma, Škapin, Srečo D.: Determination of the photocatalytic efficiency of TiO_2 coatings on ceramic tiles by monitoring the photodegradation of organic dyes. Ceram. Int. 38(2), 1611–1616 (2012)

Raimondo, M., Guarini, G., Zanelli, C., Marani, F., Fossa, L., Dondi, M.: Printing nano TiO_2 on large-sized building materials: technologies, surface modifications and functional behaviour. Ceram. Int. 38(6), 4685–4693 (2012)

Riaz, N., Chong, F.K., Dutta, B.K., Man, Z., Khan, M.S., Nurlaela, E.: Photodegradation of orange II under visible light using $Cu–Ni/TiO_2$: effect of calcination temperature. Chem. Eng. J. 185, 108–119 (2012)

Riyas, S., Krishnan, G., Mohandas, P.N.: Anatase–rutile transformation in doped titania under argon and hydrogen atmospheres. Adv. Appl. Ceram. 106, 255–264 (2007)

Shon, H., Phuntsho, S., Okour, Y., Cho, D.L., KK, S., Li, H.J, Na, S.H., Kim, J.B., Kim, J.H.: Visible light responsivetitanium dioxide (TiO_2). J. Korean Ind. Eng. Chem. 19(1), 1–16 (2008)

Siddhapara K, Shah D. (2012) J. Crystal Growth 352: 224-228.

Smitha, V.S., Manjumol, K.A., Baiju, K.V., Ghosh, S., Perumal, P., Warrier, K.G.K.: Sol–gel route to synthesize titania-silica nano precursors for photoactive particulates and coatings. J. Sol-Gel. Sci. Technol. 54, 203–211 (2010)

Sreethawong, T., Suzuki, Y., Yoshikawa, S.: Photocatalytic evolution of hydrogen over mesoporous TiO_2 supported NiO photocatalyst prepared by single-step sol–gel process with surfactant template. Int. J. Hydrogen Energy 30(10), 1053–1062 (2005)

Sun, B., Vorontsov, A.V., Smirniotis, P.G.: Role of platinum deposited on TiO_2 in phenol photocatalytic oxidation. Langmuir 19, 3151–3156 (2003)

Supha, C., Boonto, Y., Jindakaraked, M., Ananpattarachai, J., Kajitvichyanukul, P.: Long-term exposure of bacterial and protozoan communities to TiO_2 nanoparticles in an aerobic-sequencing batch reactor. Sci. Tech. Adv. Mater. 16(3), 034609 (2015)

Tsai, S.J., Cheng, S.: Effect of TiO_2 crystalline structure in photocatalytic degradation of phenolic contaminants. Catal. Today 33, 227–237 (1997)

Vegard, L.: The constitution of mixed crystals and the space occupied by atoms. Z. Phys. 5, 17–26 (1921)

Verma, A., Samanta, S.B., Bakhshi, A.K., Agnihotry, S.A.: Effect of stabilizer on structural, optical and electrochemical properties of sol–gel derived spin coated TiO_2 films. Sol. Energy Mater. Sol. Cells 88, 47–64 (2005)

Xie, Y., Yuan, C.: Photocatalysis of neodymium ion modified TiO_2 sol under visible light irradiation. Appl. Surf. Sci. 221, 17–24 (2004)